THE JOURNAL OF BIOLOGICAL CHEMISTRY
Vol. 276, No. 48, Issue of November 30, pp. 44993–45000, 2001

Printed in U.S.A.

Crystal Structure of a Soluble Form of the Intracellular Chloride Ion Channel CLIC1 (NCC27) at 1.4-Å Resolution*

Received for publication, August 14, 2001
Published, JBC Papers in Press, September 10, 2001, DOI 10.1074/jbc.M107804200

Stephen J. Harrop‡§, Matthew Z. DeMaere‡§¶, W. Douglas Fairlie‖, Tamara Reztsova‡, Stella M. Valenzuela‖, Michele Mazzanti‡‡, Raffaella Tonini**‡‡, Min Ru Qiu‖, Lucy Jankova‡, Kristina Warton‖, Asne R. Bauskin‖, Wan Man Wu‖, Susan Pankhurst‖, Terence J. Campbell§§, Samuel N. Breit§‖, and Paul M. G. Curmi‡§¶¶**

*From the ‡Initiative for Biomolecular Structure, School of Physics and the §§Department of Medicine, University of New South Wales, New South Wales 2052, Australia, the ‖Centre for Immunology, St. Vincent's Hospital and University of New South Wales, Sydney New South Wales 2010, Australia, and the **Dipartimento di Biologia Cellulare e dello Sviluppo and the ‡‡Dipartimento di Fisiologia Umana e Farmacologia, Universita "La Sapienza," 00185 Roma, Italy*

CLIC1 (NCC27) is a member of the highly conserved class of chloride ion channels that exists in both soluble and integral membrane forms. Purified CLIC1 can integrate into synthetic lipid bilayers forming a chloride channel with similar properties to those observed *in vivo*. The structure of the soluble form of CLIC1 has been determined at 1.4-Å resolution. The protein is monomeric and structurally homologous to the glutathione *S*-transferase superfamily, and it has a redox-active site resembling glutaredoxin. The structure of the complex of CLIC1 with glutathione shows that glutathione occupies the redox-active site, which is adjacent to an open, elongated slot lined by basic residues. Integration of CLIC1 into the membrane is likely to require a major structural rearrangement, probably of the N-domain (residues 1–90), with the putative transmembrane helix arising from residues in the vicinity of the redox-active site. The structure indicates that CLIC1 is likely to be controlled by redox-dependent processes.

Chloride ion channels, located both within the plasma membrane and other internal cell membranes (1, 2), are involved in diverse physiological processes. They are known to participate in the control of secretion and absorption of salt, regulation of membrane potentials, organellar acidification, and cell volume homeostasis (3). Malfunction in these channels can lead to severe disease states (4).

Chloride channels fall into several classes based on their sequence relationships. The three best characterized classes are the ligand-gated receptor channels (γ-aminobutyric acid and glycine receptors), the cystic fibrosis transmembrane conductance regulator family, and the ClC chloride ion channels (1, 2). A new class of chloride ion channel, the "chloride intracellular channels" (CLICs),[1] has recently been characterized at a molecular level. To date, there are seven members of the CLIC family: CLIC1 (NCC27) (5), CLIC2 (6), CLIC3 (7), CLIC4 (8), CLIC5 (9), p64 (10), and parchorin (11). All of these proteins exist as soluble globular proteins that can form ion channels in organellar and plasma membranes (5, 7, 8, 12–15). Five of the CLIC proteins are each composed of ~240 residues, while the longer p64 and parchorin consist of distinct amino-terminal domains followed by the 240-residue CLIC module. This module has recently been shown to share weak sequence homology with the glutathione *S*-transferase (GST) superfamily (16).

The CLIC proteins are expressed in a wide variety of tissues and appear to have diverse physiological functions. p64 is associated with kidney function (17), while CLIC1 and CLIC4 appear to have a broad tissue distribution (5, 8, 18, 19). Several CLICs interact with protein kinases (7, 11, 20). CLICs are associated with a variety of intracellular membranes including the nuclear membrane (5), the endoplasmic reticular membrane (8), large dense-core vesicles (19), mitochondria (21), trans-Golgi vesicles (22), and secretory vesicles (23). Parchorin forms the chloride channel in water-secreting cells, and it is translocated to the plasma membrane on chloride ion depletion of the extracellular medium (11). CLIC1, which is substantially nuclear in distribution, has been implicated in the control of cell division (24). A 62-kDa homologue of p64 is crucial to osteoclast function as it forms the chloride channel that facilitates the acidification of the ruffled border in bone resorption (15).

An unusual feature of the CLIC family of ion channels is that they exist in both soluble and integral membrane forms. In this they are similar to the other intracellular ion channels like the annexins and BCL-x_L as well as some of the bacterial toxins. The manner by which CLIC proteins form a transmembrane (TM) chloride ion channel remains speculative. It has been suggested that there is either one (5) or possibly two putative

* This work was supported by grants from the National Health and Medical Research Council of Australia and by the University of New South Wales Capital Grants scheme; Australian Research Council Research Infrastructure Equipment and Facilities Program grants; St. Vincent's Hospital, Sydney; Meriton Apartments Pty Ltd through a research and development syndicate arranged by Macquarie Bank Limited; New South Wales Health Research and Development infrastructure grant; and the Rebecca L. Cooper Medical Research Foundation. This work was also funded by grants from the Ministero dell'Universitá e della Ricerca Scientifica e Tecnologica (Italian Minister) and Consiglio Nazionale delle Ricerche (National Research Center) (to M. M.). The costs of publication of this article were defrayed in part by the payment of page charges. This article must therefore be hereby marked "*advertisement*" in accordance with 18 U.S.C. Section 1734 solely to indicate this fact.

The atomic coordinates and structure factors (code 1K0M, 1K0N, and 1K0O) have been deposited in the Protein Data Bank, Research Collaboratory for Structural Bioinformatics, Rutgers University, New Brunswick, NJ (http://www.rcsb.org/).

§ These authors contributed equally to this work.

¶ Supported by an Australian postgraduate award.

¶¶ To whom correspondence should be addressed: School of Physics, University of New South Wales, Sydney UNSW 2052, Australia. Tel.: 61-2-9385-4552; Fax: 61-2-9385-6060; E-mail: p.curmi@unsw.edu.au.

[1] The abbreviations used are: CLIC, chloride intracellular channel; r.m.s.d., root mean square deviation; TM, transmembrane; GST, glutathione *S*-transferase; CHO, Chinese hamster ovary.

TABLE I
Phasing statistics at 2.8 Å

Data	Cdit[a]	Complete[b]	R_{sym}[c]	Red.[d]	I/σ	R_{iso}[e]	R_{cullis}[f]	Sites[g]	PhP[h]
Native		98.0 (90.2)[i]	0.045 (0.143)	3.5	18.0 (6.5)				
Hg1	2 wk	99.9 (100)	0.057 (0.24)	7.2	23.35 (5.2)	0.42	0.55/0.42[j]	12	2.0/3.6[j]
Hg2	1 day	96.4 (96.2)	0.044 (0.15)	3.4	14.8 (6.2)	0.21	0.76/0.57	12	1.4/2.8
Hg3	3 days	96.9 (86.6)	0.047 (0.21)	3.8	21.2 (8.4)	0.41	0.49/0.45	11	3.5/2.1

[a] Soak time in 0.5 mM $HgCl_2$.
[b] Completeness of the data.
[c] $R_{sym} = \Sigma|I_i - \langle I_i \rangle|/\Sigma I_i$.
[d] Average redundancy.
[e] $R_{iso} = \Sigma|F_{PH} - F_P|/\Sigma|F_P|$.
[f] $R_{cullis} = \Sigma\|F_{PHobs}| - |F_{PHcalc}\|/\Sigma\|F_{PH}| - |F_P\|$.
[g] Number of mercury sites.
[h] Phasing power = $\Sigma|F_H|/\Sigma\|F_{PHobs}| - |F_{PHcalc}\|$.
[i] Values in parentheses refer to the high resolution shell (2.9–2.8 Å).
[j] Slash separates acentric and centric values.

TM helices (5, 10). Studies with FLAG epitope-tagged CLIC1 suggest that when it is integrated into the plasma membrane the amino terminus is on the outside, and the carboxyl terminus is on the cytoplasmic side (12). To date, nothing is known about the structure of any chloride ion channels at an atomic level.

We have solved the crystal structure of the soluble form of CLIC1 (NCC27) at 1.4-Å resolution. The structure demonstrates that CLIC1 is a structural homologue of the GST superfamily and that it has an intact glutathione (GSH) binding site. This site closely resembles that of glutaredoxin in that it appears to have a redox-active cysteine (Cys^{24}), which is capable of forming a covalent mixed disulfide with glutathione. The glutaredoxin-like GSH binding site is conserved in all CLICs suggesting that their chloride ion channel activity may be under the control of redox-active signaling molecules *in vivo*.

EXPERIMENTAL PROCEDURES

Expression and Purification of Recombinant CLIC1—A recombinant GST-CLIC1 fusion protein was expressed in *Escherichia coli* using the pGEX-4T-1 vector system and purified as described previously (5). The protein used in this study is a point mutant form of CLIC1 (E151G), which was inadvertently generated by polymerase chain reaction infidelity. Briefly, the fusion protein was immobilized on glutathione-S-Sepharose (AMRAD-Pharmacia), where it was cleaved with biotin-labeled thrombin (Novagen). The thrombin was removed with a streptavidin-agarose affinity matrix, and CLIC1 was further purified by gel filtration on a Superdex G75 column (Amersham Pharmacia Biotech) where it ran as a monomer. Protein was dialyzed and concentrated to 10–20 mg/ml using a vacuum dialysis system (Sartorius). In addition to the point mutation, the final product contained two additional residues at the amino terminus (Gly-Ser) that formed part of the thrombin cleavage site in the fusion construct (5).

Structure Determination—Crystals of CLIC1 were grown by sitting or hanging drop vapor diffusion at 4 °C by mixing equal volumes of protein (5–20 mg/ml with 0.5% *n*-octyl β-D-glucopyranoside) with reservoir buffer consisting of 14–18% polyethylene glycol monomethylether 5000, 0–30 mM ammonium sulfate, and 0.1 M sodium acetate, pH 5.0. Crystals were sensitive to temperature; hence, all manipulations were carried out at 4 °C. Crystals appeared within 1 week, after which they were transferred to a cryoprotectant by a series of transfers to a final solution consisting of reservoir buffer plus 10% polyethylene glycol 400 and 200 mg/ml glucose. Diffraction data were collected in house at 100 K on a DIP2030 imaging plate system mounted on a Nonius rotating anode generator using CuK_α radiation and focusing mirrors. Two crystal forms were produced: P1 with lattice dimensions a = 42.52 Å, b = 45.19 Å, c = 71.27 Å, α = 102.79°, β = 100.21°, and γ=110.88°; and $P2_1$ with lattice dimensions a = 46.69 Å, b = 60.93 Å, c = 90.11 Å, and β = 92.27°; they diffracted to 2.0 and 2.4 Å, respectively. A monoclinic crystal underwent a lattice transition to $P2_1$ with a = 45.18 Å, b = 55.14 Å, c = 88.96 Å, and β = 90.0° and diffracted to 1.4-Å resolution. A data set was collected at the Stanford Synchrotron Radiation Laboratory (SSRL) beamline BL-9.1 with an x-ray wavelength of λ = 0.98 Å on a MAR on-line image plate detector. A 2.3 Å data set was collected from the same crystal to ensure data completeness at low resolution. All data were processed using the programs DENZO and SCALEPACK (25). Rotation functions (26) showed that all crystal forms had a noncrystallographic two-fold axis with two molecules in the asymmetric unit.

Several derivative data sets were collected from the $P2_1$ β = 92° crystal form by soaking it in 0.5 mM $HgCl_2$ for between 2 h and 2 weeks at 4 °C (Table I). Twelve mercury sites with varying occupancies were located by difference Patterson and difference Fourier methods using the CCP4 suite of programs (27). Phases generated from three mercury derivatives (varying in soak time) were used to generate a DM (28) modified map at 2.8-Å resolution (Table I). The map was of sufficient quality to allow the main chain to be traced using the program O (29). A model was built consisting of residues Pro^6–Leu^{148} and Lys^{166}–Lys^{241}. This model was then used as a molecular replacement model for the 1.4-Å resolution $P2_1$ β = 90° data set. The program wARP was used to refine the phases (30). The wARP map showed clear density for all residues from Pro^6 to Lys^{241} for each monomer in the asymmetric unit. The model was built in program O and refined using REFMAC5 (31). wARP was then used to build in water molecules. A similar procedure was used to solve the structure of the 2.0-Å resolution P1 data set.

For the 1.4-Å resolution data, the final model consists of residues Pro^6 to Lys^{241} for each monomer in the asymmetric unit plus 660 water molecules. The crystallographic *R*-factor is 0.138 with *R*-free 0.178 (32). The two monomers in the asymmetric unit are nearly identical with the A monomer slightly more ordered as evidenced by B-factors and difference maps. Differences are observed around Pro^{90}, which is cis in the A monomer but appears to be in two states (cis and trans) in the B monomer. This alternate conformer of Pro^{91} results in the presence of two states for helices h1 and h3 in the B monomer. This may indicate some plasticity in the molecule, which is described under "Results and Discussion." Another region of flexibility is the extended loop from Pro^{147} to Gln^{164}. This has several regions of poor side chain density in the A monomer, and the density is generally weaker in the B monomer. The point mutation E151G resides in this loop. Table II gives data collection and refinement statistics for the high resolution crystal form. Coordinates and structure factors have been deposited with the PDB (accession code 1K0M). All macromolecular figures were made using the program SETOR (33).

Structure of the Glutathione Complex—Crystals of the β = 92° form were soaked with 5 mM GSSG in stabilization buffer. 1.75-Å resolution data sets were collected at SSRL (at 100 K) using a Quantum-4 CCD camera (ADSC) for native and GSSG-soaked CLIC1 crystals. These were processed as per the native form (Table II). The structure of the native state was determined by molecular replacement using the refined 1.4 Å structure as a starting model. In the β = 92° crystal form, monomer B is disordered compared with monomer A. The crystal structure was modeled by TLS refinement as implemented in the program REFMAC5 (31) followed by coordinate and B-factor refinement using REFMAC5 as per the 1.4 Å structure. The final model consisted of residues Pro^6–Pro^{147} and Arg^{165}–Lys^{241} in monomer A and residues Pro^6–Cys^{89}, Arg^{92}–Leu^{99}, Ser^{103}–Pro^{147}, and Arg^{165}–Lys^{241} in monomer B. $2F_o - F_c$ maps showed excellent electron density for monomer A with

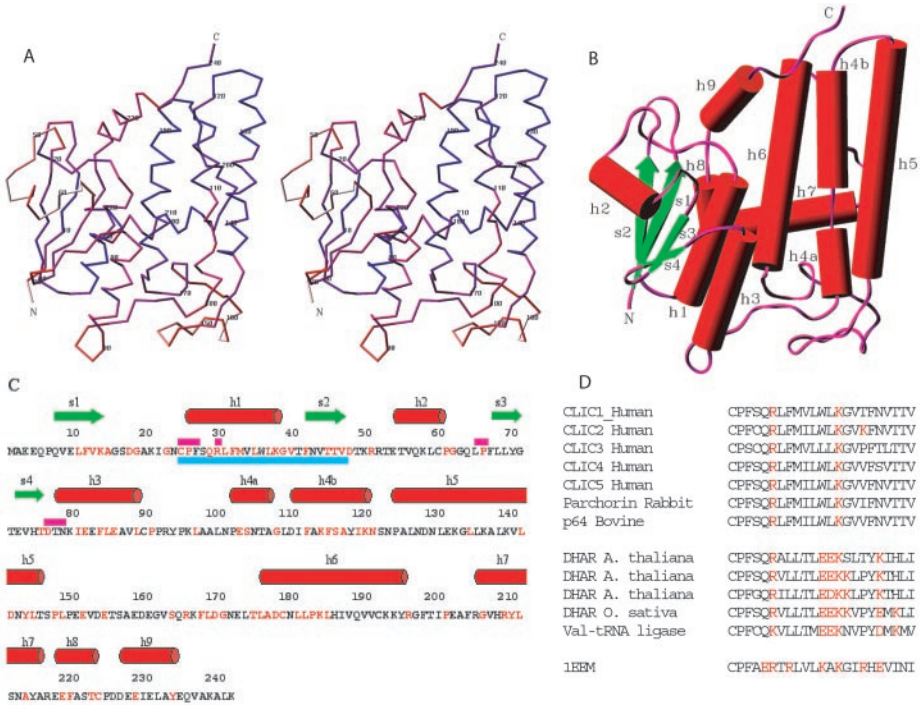

FIG. 1. **The structure of CLIC1.** *A*, a stereo diagram showing a C_α trace of CLIC1 A monomer from the 1.4 Å data set. The N-domain is on the *left-hand side* with the C-domain on the *right*. The GSH site is at the *top* of the molecule in the interdomain cleft. The backbone has been colored by B-factor with *blue* for low and *red* for high. *B*, a schematic showing the arrangement of secondary structural elements in CLIC1. The view is similar to *A*. *C*, the sequence of CLIC1 with secondary structural elements marked as per *B*. All residues that are strictly conserved in all CLICs are shown in *red*. The *pink bars* indicate the residues that are implicated in GSH binding. The *blue bar* shows the putative transmembrane helix of the integral membrane form of CLIC1. *D*, the alignment of the seven CLIC sequences in the region of the putative TM helix (Cys^{24}–Val^{46}). Also shown are the sequences of the closely related GSH-dependent dehydroascorbate reductases and the Ω class GST. Charged residues are shown in *red*.

broader density for portions of monomer B due to the angular disorder. This is reflected in the relatively small number of well defined water molecules and the high crystallographic *R*-factors. Refinement statistics are shown in Table II. Coordinates and structure factors have been deposited with the PDB (accession code 1K0O).

To determine the effect of the soaking GSSG into the crystals, difference Fourier maps were generated by subtracting the experimental amplitudes and calculating phases based on the refined $\beta = 92°$ native structure. The only difference density observed at 4σ was in the vicinity of Cys24 in each monomer. Difference electron density was stronger and showed better definition in monomer A, in keeping with the protein density. The structure of the glutathione complex was solved and refined as per the native, $\beta = 92°$ where glutathione atoms were excluded from initial stages of refinement. Finally, glutathione was docked into the difference density in monomer A only and the refined as per the native structure (Table II). As per the native form, monomer A showed excellent electron density while monomer B showed regions with broad features. This is reflected in the refinement statistics (Table II). Coordinates and structure factors have been deposited with the PDB (accession code 1K0N).

GSH Binding Studies—To determine the number of covalent glutathione-CLIC1 adducts and their respective equilibrium constants, K_{ox} = ([RSSG][GSH])/([RSH][GSSG]), CLIC1 (1 mg/ml in 100 mM potassium phosphate buffer, pH 7.0) was incubated overnight at 4 °C with various ratios of [GSH]/[GSSG] from 1:10 to 2:1 (Table IV). In each case the concentration of GSSG was 5 mM except in the 2:1 sample where the concentration of GSH was 5 mM. The protein was then dialyzed against 10 mM Tris-HCl, pH 8.0 and analyzed by mass spectrometry on a matrix-assisted laser desorption ionization/time of flight mass spectrometer (Applied Biosystems Voyager DE-STR) in positive ion mode using a caffeic acid matrix with external calibration using β-lactoglobulin-A (operated by Dr. Anne Poljak at the Ray Williams Biomedical Mass Spectrometry Facility at the University of New South Wales, Sydney). Each sample was analyzed in duplicate, and the percentages of glutathione-adducted CLIC1 molecules were determined by calculating the relative areas under each peak in the spectrum for the doubly charged species as this gave greater resolution than the singly charged species. The mass spectrometry data was fitted to four and six independent binding site models with individual equilibrium constants, K_{ox}, which were evaluated by minimizing the χ^2 between the distribution of observed and calculated oxidized species.

Electrophysiology—Single-channel recordings from lipid bilayers were obtained using the tip-dip method (34). In brief, patch-clamp pipettes (Garner Glass 7052) were made using a P97 Sutter puller (Novato, CA) decorated with Sylgard (Dow Corning) and fire-polished to a tip diameter of 1–1.5 μm and 5–7-megaohm resistance. The same solution (140 mM KCl, 10 mM Hepes, pH 6) was used both in the bath and in the pipette. As soon as the pipette tip reached the bath solution a phospholipid monolayer (phosphatidylcholine; Avanti Polar Lipids, Inc., Birmingham, AL) was spread on the surface. Repetitive solution dipping of the electrode was continued until the pipette resistance reached a value higher than 5 gigaohms. Purified recombinant CLIC1 protein was then added to the bath to reach a final concentration of 2 μg/ml. Axopatch 1D and pCLAMP 7 (Axon Instruments, Inc., Novato, CA) were used to record and analyze single-channel currents. Current recordings were digitized at 5 kHz and filtered at 800 Hz. As a control, we performed patch-clamp electrophysiology on inside-out patches of a CLIC1-expressing CHO cell line using standard methods as reported previously (12).

RESULTS AND DISCUSSION

Structure of CLIC1—The structure of the soluble form of CLIC1 (point mutant E151G) has been determined in two crystal forms at 1.4-Å ($P2_1$, $\beta = 90°$) and 1.75-Å ($P2_1$, $\beta = 92°$) resolution, respectively (Fig. 1, see Tables I and II for details regarding structure determination and refinement). In each crystal form, the protein is monomeric albeit with two molecules in the asymmetric unit. In the 1.4 Å structure, clear electron density was seen for all residues from Pro^6 to Lys^{241}, while in the second form, residues Leu^{148}–Arg^{165} are disordered. For the most part, all structures are identical (r.m.s.d. of 0.34 Å between the A and B monomers of the 1.4 Å structure compared with r.m.s.d. of 0.5 Å between the A monomers in the $\beta = 90°$ and $\beta = 92°$ crystal forms) with slight alterations observed in the loop region (Pro^{147}–Gln^{164}) at the foot of the molecule (Fig. 1, *A* or *B*, *bottom right*). This region extends from the body of the protein, and its structure is likely to be more susceptible to alterations caused by crystal packing. There is also evidence for plasticity within the structure (see below).

Relationship between the CLICs and the GST Superfamily—Ψ-Blast searches (35) of the nonredundant protein sequence data bases show that the CLIC proteins are related to the GST superfamily of proteins (36, 37) as shown previously (16). The closest relatives are the plant GSH-dependent dehydroascorbate reductases (25% identity over 233 residues for putative dehydroascorbate reductase from *Arabidopsis thaliana*; GenBank™ accession number AAF98403) as well as a domain of the valyl tRNA ligase (25% identity over 212 residues for putative ligase from *A. thaliana*; PIR code T51503). The closest

TABLE II
Native data collection and refinement statistics

Glutathione			Yes
Space group	$P2_1$	$P2_1$	$P2_1$
Lattice parameters			
a =	45.18	46.41	46.51
b =	55.14	60.31	60.36
c =	88.96	89.43	89.63
β =	90.0	92.41	92.50
Number of crystals	1	1	1
Number of measured reflections	259,290	212,823	208,943
Number of unique reflections	81,729	48,235	44,693
Maximum resolution (Å)	1.4	1.75	1.80
Outer shell (Å)	(1.42–1.40)	(1.84–1.75)	(1.90–1.80)
Completeness of data (%)	94.1 (94.0)	98.2 (97.0)	98.0 (93.9)
I/σ	28 (6.5)	9.9 (1.6)	9.6 (3.4)
R_{sym}	0.03 (0.08)	0.044 (0.46)	0.046 (0.20)
Number of protein atoms	3,732	3,450	3,506
Number of water molecules	660	133	67
Crystallographic *R*-factor	0.138	0.243	0.253
R_{free}	0.178	0.272	0.285
r.m.s.d. bond lengths[a] (Å)	0.018	0.017	0.012
r.m.s.d. bond angles[a] (°)	1.7	1.7	1.3
Ramachandran plot[b] (%)			
Most favored region	94.0	92.9	92.0
Additionally allowed	5.6	6.8	7.2
Generously allowed	0.4	0.3	0.8
Disallowed	0	0	0

[a] From REFMAC5 (31).
[b] From PROCHECK (53).

sequence-related proteins of known structure are the GST from *Zea mays* (PDB code 1AW9; 21% identity) (38) and the Ω class GST (PDB code 1EEM; 16% identity) (39).

The structure of the soluble form of CLIC1 indicates that it belongs to the GST superfamily (Fig. 1) and closely resembles that of the Ω class GST (39). The molecule is flat (55 × 52 × 23 Å) consisting of two discrete domains, which we refer to as the N- and C-domains (Fig. 1). The N-domain (residues 1–90) has a thioredoxin fold that consists of a four-stranded mixed β-sheet plus three α-helices, while the C-domain is all helical, closely resembling the Ω class GST with two exceptions: the insertion of a highly negatively charged loop region (Pro^{147}–Gln^{164}) at the foot of the molecule and the position of the carboxyl-terminal helix h9 (Fig. 2). Table III presents a least squares structural comparison between CLIC1 and three sequence-related GSTs. In all cases, the N-domains are very similar, while only the C-domain of the Ω GST is close to CLIC1. CLIC1 and Ω GST are distinct in that helices h4 and h5 are very straight, facilitating significant structural alignment (Fig. 2). In contrast to the GSTs, where all known members are dimeric (36, 37), CLIC1 is monomeric both in the crystals and in solution as determined by size-exclusion chromatography (data not shown).

The long loop between helices h5 and h6 at the foot of CLIC1 (Pro^{147}–Gln^{164}) is a distinctive feature of the CLICs. It is highly negatively charged with seven acidic residues between Pro^{149} and Glu^{160} in CLIC1 giving a net charge of −7 (*cf.* a net negative charge of 6 in CLIC4 and p64, 5 in CLIC2, 5 in parchorin, and 3 in CLIC3). This loop is spatially adjacent to the loop linking the two domains, and it may be important in protein-protein interactions.

Plasticity in the CLIC1 Structure—The N- and C-domains of CLIC1 are linked by a proline-rich loop from Cys^{89} to Asn^{100}, which joins helices h3 to h4a (Fig. 1). The region between Pro^{90} and Pro^{94} forms a sharp turn with Pro^{91} in a cis conformer. This segment has a WW domain binding consensus sequence, Pro-Pro-Xaa-Tyr (40). In the B monomer of the 1.4-Å resolution structure, the electron density map shows that CLIC1 exists in two conformations in the vicinity of the proline-rich domain-connecting loop. First, Pro^{91} is trans in the minor conformer.

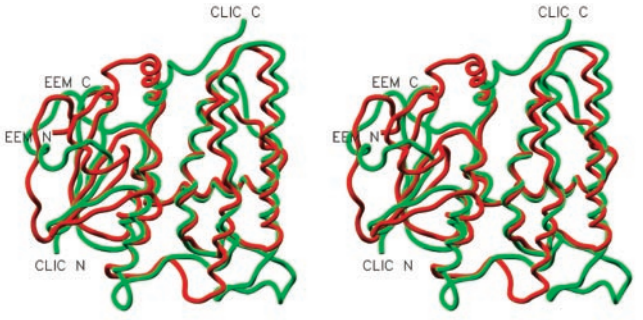

FIG. 2. **A comparison of the structure of CLIC1 with that of Ω GST.** The figure shows a stereogram of the superposition of the CLIC1 structure (*green*) with that of the Ω class GST (*red*) (39). The view is similar to that shown in Fig. 1, *A* and *B*.

TABLE III
Structural comparison between CLIC1 and sequence-related GSTs

Protein	PDB code	r.m.s.d.		
		Overall	N-domain	C-domain
		Å (no. of C_α atoms)		
GST Ω	1EEM	2.08 (163)	1.58 (67)	1.76 (110)
GST II	1GNW[a]	1.59 (88)	1.22 (62)	2.06 (73)
GST	1AW9	1.96 (91)	1.59 (62)	1.91 (21)

[a] Ref. 54.

This results in a second conformer for the proline-rich loop as well as helices h1 and h3. We have modeled the alternative conformation for the helices, and note that each is displaced by 1.0–1.5 Å from the main conformer and tilted by 4.4 and 1.9° for helices h1 and h3, respectively. These two N-domain helices form the interface between the N- and C-domains. Thus, the observation of two conformations indicates that the domain interface is somewhat plastic and that there is a connection between the conformation of the proline-rich linker and the relative orientation of the two domains. This region of the molecule may be susceptible to structural alterations as part of its function *in vivo*.

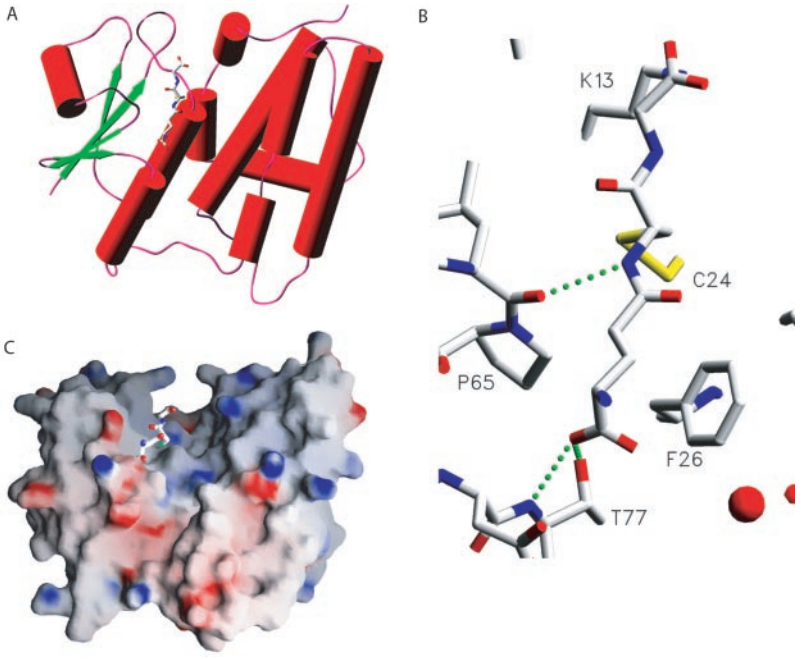

FIG. 3. **The structure of the glutathione·CLIC1 complex.** *A* shows the location of bound glutathione on the schematic representation of CLIC1. *B* shows a close-up of the glutathione site in a similar orientation as *A*. *C* shows the electrostatic potential on the molecular surface of glutathione-bound CLIC1 oriented approximately as per Fig. 1*B*. Glutathione can be seen at the edge of a slot at the top of the molecule, which is surrounded by the basic lobes of the N and C domains. The electrostatic potential and molecular surface were computed using the program GRASP (52). Note that the negatively charged foot loop is absent from *A* and *C* due to its disorder in this crystal form.

Glutathione Binding Site and the Structure of the CLIC1·Glutathione Complex—The N-domain has a well conserved glutaredoxin-like site for covalently interacting with GSH. The amino terminus of helix h1 has the conserved Cys-Pro-(Phe/Ser)-(Ser/Cys) motif (Fig. 1*C*), which corresponds to Cys-Pro-(Phe/Tyr)-(Cys/Ser) in the glutaredoxins (41). The thiol of Cys^{24} in CLIC1 is likely to be a highly reactive thiolate with a low pK_a due to its position at the amino terminus of helix h1 (42) and the basicity of conserved Arg^{29} (which corresponds to the conserved Lys/Arg in glutaredoxins) (41). Other conserved portions of the GSH binding site include the cis-proline Pro^{65} and Asp^{76} (marked with a *pink bar* on the sequence in Fig. 1*C*). Thus, CLIC1 and the CLICs are likely to be GSH-dependent redox-active proteins. Two of the CLICs (CLIC2 and CLIC3) also have the second cysteine of the thioredoxin/glutaredoxin redox motif Cys-Xaa-Xaa-Cys (Fig. 1*D*). Thus, CLIC2 and CLIC3 could reduce a substrate at the expense of forming a disulfide bond between the two cysteines of the thioredoxin/glutaredoxin motif. This would then be reduced by glutathione binding as per glutaredoxin.

Oxidized glutathione (GSSG) was soaked into the $P2_1$ β = 92° CLIC1 crystals. Difference electron density maps showed prominent peaks (contoured at 4σ) adjacent to Cys^{24} in both monomers with no other significant peaks in the difference map. This density corresponds to CLIC1-bound glutathione (Fig. 3). Clear electron density was observed for the γ-glutamyl and cystyl portions of glutathione, while the glycyl portion appears to be in at least two conformations with the cystyl ψ angle at ~0 and 180°, respectively. Glutathione binding has induced only small changes in the protein structure (r.m.s.d. of 0.29 Å between monomer A in apo and glutathione-bound β = 92° crystal forms).

Glutathione appears to be covalently attached to Cys^{24} via a disulfide bond; however, the electron density indicates that the glutathione cystyl side chain adopts both the gauche$^-$ and gauche$^+$ rotamers (χ_1 = 60 and −60°) with the former being the major conformer. The γ-glutamyl moiety is positioned in a groove formed by the backbone of the loop joining helix h2 with β-strand s3 and the side chain of Phe^{26} (Fig. 3, *A* and *B*). The backbone amide of the glutathione cystyl moiety forms a hydrogen bond with the carbonyl of Leu^{64}, while the carboxyl group of the γ-glutamyl moiety is hydrogen-bonded to the backbone and side chains of the loop joining β-strand s4 to helix h3 (Fig. 3*B*).

The site is more open than that observed in GSTs with fewer interactions between glutathione and the protein. In our structure, we see no interactions between CLIC1 and either the terminal nitrogen of the γ-glutamyl moiety or the cystyl carbonyl group. These interactions are present in all structures of GST·glutathione complexes. In all GSTs, with the exception of the Ω class GST, the γ-glutamyl nitrogen ligand comes from the partner monomer in the GST dimer.

The glutathione binding site of CLIC1 differs from typical eukaryotic GST glutathione sites in several other key aspects. In GSTs, the protein not only binds to GSH, but it is designed to ensure the nucleophilicity of the sulfur atom of GSH. This is achieved by both the positioning of the GSH sulfur and the hydrogen bond donors (tyrosine or serine residues conserved in GSTs) that are poised to ensure that the GSH sulfur is a reactive thiolate ion (36, 37). In contrast, the CLIC1 GSH site appears to be designed to ensure the nucleophilicity of the Cys^{24} sulfur atom as in the glutaredoxins. The Ω class GST is more like CLIC1 than other eukaryotic GSTs, which is consistent with its lack of activity toward most GST substrates (39).

A molecular surface representation of CLIC1 shows that the bound glutathione lies to one side of a distinct slot that separates the N- and C-domains (Fig. 3*C*). This slot is potentially a substrate binding site for the target molecule of the CLIC1 redox activity. It differs from the substrate site in the Ω class GST (and other GSTs) in that it is more open and elongated (*cf.* Fig. 2). The slot is also basic, which is primarily due to clusters of arginines and lysines at the carboxyl termini of helices h4 and h6 (top of the C-domain) and at the carboxyl termini of β-strands s1 and s2 (top of the N-domain). The overall charge distribution of CLIC1 is asymmetric as can be seen from the electrostatic potential on the protein surface (Fig. 3*C*). Thus, CLIC1 has a strongly dipolar character with the dipole moment pointing up out of the GSH binding site/slot region. This is similar to some thioredoxins and glutaredoxins and may be related to substrate specificity (43).

Glutathione Binding to CLIC1 in Solution—Noncovalent binding of GSH to CLIC1 appears to be weak. CLIC1 does not bind to GSH-agarose gels (with the GSH conjugated either by its sulfhydryl or its amino terminus). Preliminary GSH binding

TABLE IV
Formation of glutathione-CLIC1 adducts

[GSH]/[GSSG]	Observed glutathione bound per CLIC1				
	0	1	2	3	4
	% total protein (% calculated on six-site model)				
0.0	6	13	40	29	12
0.1	13 (3)[a]	15 (21)	34 (36)	23 (28)	16 (11)
0.2	16 (9)	42 (40)	31 (34)	11 (13)	0 (3)
0.5	41 (31)	44 (49)	15 (17)	0 (3)	0 (0)
1.0	47 (51)	41 (41)	12 (7)	0 (1)	0 (0)
2.0	59 (69)	32 (28)	8 (2)	0 (0)	0 (0)

[a] Numbers in parentheses are % of total protein calculated on the six-site model.

studies using isothermal titration calorimetry have not been able to detect any noncovalent GSH binding up to 10 mM GSH indicating that the dissociation constant is greater than 10 mM. This contrasts with the strong binding of GSH to GSTs ($k_d \sim \mu$M) (36). The weak binding is consistent with the more open glutathione binding site observed in the crystal structure.

Covalent complexes between GSH and CLIC1 can be formed under a variety of oxidizing conditions. Mass spectrometry analysis shows that at least four glutathiones can covalently bind per CLIC1 monomer (Table IV). We have fitted the data to models consisting of four and six reactive thiols per CLIC1 monomer with the latter model giving a better fit (lower χ_ν^2). For both models, one protein sulfhydryl is significantly more reactive than the rest, which are indistinguishable from each other. The six-site model gave a solution with an equilibrium constant $K_{ox} = 0.60$ for the main site and $K_{ox} = 0.041$ for the remaining sites ($\chi_\nu^2 = 1.22$), while for the four-site model $K_{ox} = 0.57$ for the main site and $K_{ox} = 0.076$ for the remaining sites ($\chi_\nu^2 = 1.49$). The distribution of glutathione-modified CLIC1 species predicted by the six-site model is compared with the observed distribution in Table IV. In summary, both models show that CLIC1 has a single reactive cysteine, which is distinct from the other cysteines.

Formation of Chloride Ion Channels by CLIC1 in Lipid Bilayers—The fact that CLIC1 (and the CLICs) are cytoplasmic as well as membrane proteins in distribution and appear to contain the domains of a functional GSH-dependent redox protein structurally related to the GST superfamily raises the question as to whether CLIC1 is a just a regulatory element controlling an integral membrane ion channel. Several lines of evidence indicate that the CLIC proteins exist in a true integral membrane form. First, the CLIC4 fraction that partitions in the membrane is resistant to alkali extraction (8, 18, 22). Second, immunogold electron microscopy using an antibody generated against an 18-amino acid peptide from the carboxyl terminus of p62 shows that the protein is localized to the osteoclast ruffled border membrane with 66% of the gold beads within one bead diameter of the membrane (15). Also, our previous studies using epitope-tagged CLIC1-transfected CHO cells indicate that CLIC1 is a transmembrane protein that directly forms part of the ion channel whose conductance is blocked by a monoclonal antibody to the epitope tag. Further, we could deduce that the amino terminus projects outward, and the carboxyl terminus projects inward from the plasma membrane (12), indicating that the protein spans the membrane an odd number of times. Finally, a recent study (13) has shown that recombinant CLIC1 can form chloride ion channels in lipid bilayers, but the characteristics of the channels differed from those measured in CHO cells transfected with CLIC1 (5, 12).

To evaluate the ability of our purified recombinant CLIC1 to form ion channels we used the tip-dip electrophysiological technique (34, 44). Following bilayer formation on the patch pipette, we added the purified recombinant CLIC1 to the bath

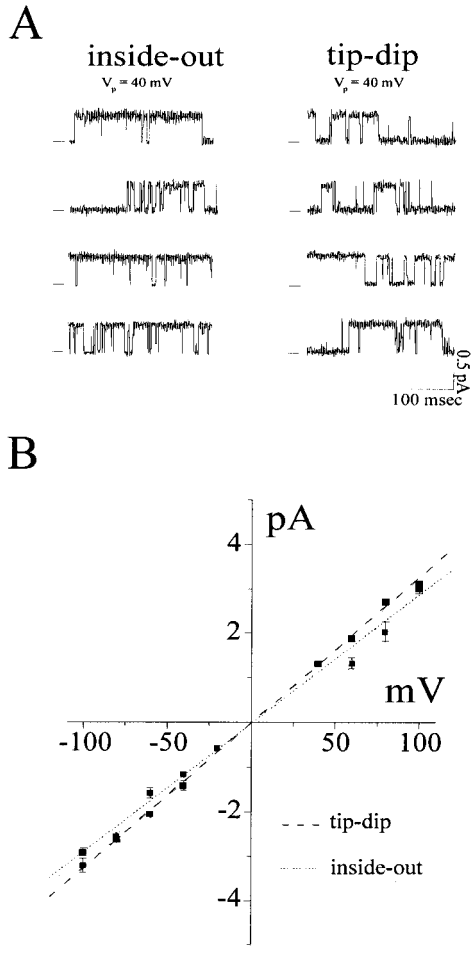

FIG. 4. **Electrophysiology of purified recombinant CLIC1.** Comparison between inside-out experiments using CLIC1-transfected CHO cells and isolated CLIC1 protein inserted in lipid bilayers (*tip-dip*). *A*, single-channel current recordings at 40-mV pipette voltage obtained in inside-out (*left*) and tip-dip (*right*) configuration. *B*, single-channel current/voltage relationships from five experiments in each configuration. Experimental points were fitted by linear regression ($p = 0.001$). Single-channel conductances are 32.2 ± 0.067 and 28.82 ± 0.012 picosiemens for lipid bilayer and inside-out experiments, respectively.

solution. We were able to see current events on almost every trial (95%). The CLIC1-mediated chloride conductance in lipid bilayers is very similar to that which we have reported in the inside-out configuration for CLIC1 in transfected CHO cells (12). This similarity is demonstrated directly in Fig. 4*A*. Current traces at the same potential (40 mV in the recording pipette) are shown for inside-out (*left*) and tip-dip (*right*) patch-clamp configuration. In Fig. 4*B*, we superimpose the current/voltage plots obtained from five experiments in each recording mode. The conductances, in equimolar 140 mM KCl, were 31.2 ± 1.5 picosiemens for tip-dip and 29.6 ± 1.9 picosiemens for inside-out experiments.

Transmembrane Chloride Ion Channel Formation—Sequence analyses of all CLIC proteins have identified a 23-residue segment (from Cys^{24} to Val^{46} in CLIC1) that is likely to form a TM helix in the channel form of the protein (5, 7–10, 19, 21, 22). Experimental support for this hypothesis also comes from proteinase K digestion studies of CLIC4 in endoplasmic reticulum vesicles that show that the amino terminus is on the luminal side and that approximately the first 50 residues (6.2-kDa band on SDS-polyacrylamide gel electrophoresis) are protected from proteolysis (8). An alignment of the CLIC sequences between Cys^{24} and Val^{46} (CLIC1 numbering) shows that this region may form a TM helix with Arg^{29} and Lys^{37}

(plus Lys^{40} in CLIC2) lining one face of the helix (Fig. 1*D*). The central 10 amino acids (Leu^{30}–Val^{39}) are nonpolar (except Lys^{37}), while the flanking six to seven residues are more polar in character with two conserved phenylalanines (Phe^{26} and Phe^{41}). This pattern is typical for transmembrane helices (45). The basic residues may confer chloride ion selectivity to the channel, which would need to be formed from CLIC multimers.

In our structure, the putative TM helix residues form helix h1 and β-strand s2 of the N-domain (Fig. 1). These structural elements are exposed on one face of the molecule, and the nonpolar nature of the sequence results in a hydrophobic surface patch formed by helix h1 and β-strand s2. This surface is not hydrophobic in the proteins that are most closely related in sequence to the CLICs (plant GSH-dependent dehydroascorbate reductases and the Ω class GST) (Fig. 1*D*). In these non-CLIC proteins, the carboxyl-terminal end of helix h1 and the exposed surface of β-strand s2 contain several additional charged residues. The nonpolarity of helix h1 and β-strand s2 in the CLICs distinguish them from other members of the GST superfamily.

For residues Cys^{24}–Val^{46} to form a TM helix in the channel form of CLIC1, the N-domain must undergo a radical unfolding and refolding. The rearrangement of helix h1 and β-strand s2 is likely to result in a complete rearrangement of the remainder of the N-domain. We note that it is possible that CLIC1 forms an integral membrane channel via a different mechanism. However, all insertion mechanisms are likely to involve major structural changes, the nature of which must await the results of further experimentation.

Potential Modes of Regulation of CLIC1 Ion Channel Activity—The intact glutathione binding site along with the conserved Cys^{24} in what is likely to be a redox-active state suggest that CLIC1 activity is regulated by redox processes. In the cytoplasm, GSH is present at ~1–10 mM, and the conditions are strongly reducing ([GSH]/[GSSG], ~300) (46). Thus, the soluble form of CLIC1 is likely to be free of glutathione, and Cys^{24} is likely to be in a reduced state. Reactive oxygen species (*e.g.* H_2O_2) or reactive nitrogen species (*e.g.* NO), which are known to be cellular signaling molecules (47, 48), are likely to alter the resting state of soluble CLIC1. Whether this results in the insertion of soluble CLIC1 into the membrane or controls channel activity by other means must await further experimentation.

It is possible that CLIC1 and other CLICs use the GSH site for targeting the chloride channel to a particular subcellular location. The CLICs may bind to GSH-modified proteins by recognizing the mixed disulfide. It is interesting in this regard that CLIC5 forms an actin-containing complex (9), and that actin is a major GSH-modified intracellular protein (49).

Action of Inhibitors—The discovery that the CLICs are members the GST superfamily is not entirely surprising. As well as predictions based on sequence similarity, p64, the first identified CLIC, was purified and characterized by its ability to bind the chloride channel inhibitor IAA-94. This compound was based on ethacrynic acid, which is a known GST-binding molecule (17, 50). In fact, the affinity purification experiments that first isolated p64 concurrently isolated a GST (51).

Ethacrynic acid binds to GST in the (hydrophobic) electrophilic substrate site ("H-site"), which is adjacent to the GSH binding site (37). In GSTs, the H-site is formed by the loop connecting β-strand s1 to helix h1 (the "floor") and helix h4 plus the carboxyl terminus (the "walls") and helix h9 (the "lid"). This corresponds to the more open and elongated slot seen in CLIC1 (Fig. 3*C*). Due to its structural homology to ethacrynic acid, IAA-94 is likely to bind to the CLIC proteins in the slot (it has been shown to be displaced by ethacrynic acid in bovine retinal cortex vesicles (50)). Given the proximity of the slot to the GSH binding site, the mechanisms of GSH and IAA-94 in CLIC1 are likely to be related.

Mode of Action of CLIC Family Chloride Ion Channels—Our findings result in the following picture of CLIC1 and, by homology, the CLIC family in general. The proteins exist in two forms: a soluble form that has a GST fold and a transmembrane form where the amino terminus is on one side of the membrane and the carboxyl terminus is on the opposite side of the membrane. In the soluble form, the protein has a well formed GSH binding site, resembling that of glutaredoxin, which can form a covalent complex with glutathione under oxidizing conditions via Cys^{24}. In a resting cell, the soluble form of the protein is likely to be reduced and free of GSH; however, this state may be altered by the action of redox-active molecules (such as NO and H_2O_2). In the integral membrane form, the CLIC1 redox-active site is likely to be disrupted since Cys^{24} is at the amino terminus of the putative TM helix. The equilibrium between the soluble and integral membrane forms of CLIC1 may be controlled via a GSH-dependent redox mechanism *in vivo*.

Acknowledgments—We thank Gary Keenan for excellent technical support in numerous aspects of the project. We thank SSRL for access to the synchrotron facilities and for excellent support staff.

REFERENCES

1. al-Awqati, Q. (1995) *Curr. Opin. Cell. Biol.* **7,** 504–508
2. Jentsch, T. J., and Gunther, W. (1997) *Bioessays* **19,** 117–126
3. Strange, K., Emma, F., and Jackson, P. S. (1996) *Am. J. Physiol.* **270,** C711–C730
4. al-Awqati, Q. (1995) *Science* **269,** 805–806
5. Valenzuela, S. M., Martin, D. K., Por, S. B., Robbins, J. M., Warton, K., Bootcov, M. R., Schofield, P. R., Campbell, T. J., and Breit, S. N. (1997) *J. Biol. Chem.* **272,** 12575–12582
6. Heiss, N. S., and Poustka, A. (1997) *Genomics* **45,** 224–228
7. Qian, Z., Okuhara, D., Abe, M. K., and Rosner, M. R. (1999) *J. Biol. Chem.* **274,** 1621–1627
8. Duncan, R. R., Westwood, P. K., Boyd, A., and Ashley, R. H. (1997) *J. Biol. Chem.* **272,** 23880–23886
9. Berryman, M., and Bretscher, A. (2000) *Mol. Biol. Cell* **11,** 1509–1521
10. Landry, D., Sullivan, S., Nicolaides, M., Redhead, C., Edelman, A., Field, M., al-Awqati, Q., and Edwards, J. (1993) *J. Biol. Chem.* **268,** 14948–14955
11. Nishizawa, T., Nagao, T., Iwatsubo, T., Forte, J. G., and Urushidani, T. (2000) *J. Biol. Chem.* **275,** 11164–11173
12. Tonini, R., Ferroni, A., Valenzuela, S. M., Warton, K., Campbell, T. J., Breit, S. N., and Mazzanti, M. (2000) *FASEB J.* **14,** 1171–1178
13. Tulk, B. M., Schlesinger, P. H., Kapadia, S. A., and Edwards, J. C. (2000) *J. Biol. Chem.* **275,** 26986–26993
14. Edwards, J. C., Tulk, B., and Schlesinger, P. H. (1998) *J. Membr. Biol.* **163,** 119–127
15. Schlesinger, P. H., Blair, H. C., Teitelbaum, S. L., and Edwards, J. C. (1997) *J. Biol. Chem.* **272,** 18636–18643
16. Dulhunty, A., Gage, P., Curtis, S., Chelvanayagam, G., and Board, P. (2001) *J. Biol. Chem.* **276,** 3319–3323
17. Landry, D. W., Akabas, M. H., Redhead, C., Edelman, A., Cragoe, E. J., Jr., and Al-Awqati, Q. (1989) *Science* **244,** 1469–1472
18. Tulk, B. M., and Edwards, J. C. (1998) *Am. J. Physiol.* **274,** F1140–F1149
19. Chuang, J. Z., Milner, T. A., Zhu, M., and Sung, C. H. (1999) *J. Neurosci.* **19,** 2919–2928
20. Edwards, J. C., and Kapadia, S. (2000) *J. Biol. Chem.* **275,** 31826–31832
21. Fernandez-Salas, E., Sagar, M., Cheng, C., Yuspa, S. H., and Weinberg, W. C. (1999) *J. Biol. Chem.* **274,** 36488–36497
22. Edwards, J. C. (1999) *Am. J. Physiol.* **276,** F398–F408
23. Redhead, C., Sullivan, S. K., Koseki, C., Fujiwara, K., and Edwards, J. C. (1997) *Mol. Biol. Cell* **8,** 691–704
24. Valenzuela, S. M., Mazzanti, M., Tonini, R., Qui, M. R., Warton, K., Musgrove, E. A., Campbell, T. J., and Breit, S. N. (2000) *J. Physiol.* **529,** 541–552
25. Otwinowski, Z., and Minor, W. (1997) *Methods Enzymol.* **276,** 307–326
26. Navaza, J. (1994) *Acta Crystallogr. Sect. D Biol. Crystallogr.* **50,** 157–163
27. Collaborative Computing Project No. 4 (1994) *Acta Crystallogr. Sect. D Biol. Crystallogr.* **50,** 760–763
28. Cowtan, K. (1994) *Joint CCP 4 and ESF-EACBM Newsletter on Protein Crystallography* **31,** 34–38
29. Jones, T. A., Zou, J. Y., Cowan, S. W., and Kjeldgaard, M. (1991) *Acta Crystallogr. Sect. A* **47,** 110–119
30. Lamzin, V. S., and Wilson, K. S. (1993) *Acta Crystallogr. Sect. D Biol. Crystallogr.* **49,** 129–149
31. Murshudov, G. N., Vagin, A. A., and Dodson, E. J. (1997) *Acta Crystallogr. Sect. D Biol. Crystallogr.* **53,** 240–255
32. Brunger, A. T. (1992) *Nature* **355,** 472–475
33. Evans, S. V. (1993) *J. Mol. Graph.* **11,** 134–138
34. Coronado, R., and Latorre, R. (1983) *Biophys. J.* **43,** 231–236
35. Altschul, S. F., Madden, T. L., Schaffer, A. A., Zhang, J., Zhang, Z., Miller, W., and Lipman, D. J. (1997) *Nucleic Acids Res.* **25,** 3389–3402

36. Wilce, M. C., and Parker, M. W. (1994) *Biochim. Biophys. Acta* **1205,** 1–18
37. Armstrong, R. N. (1997) *Chem. Res. Toxicol.* **10,** 2–18
38. Neuefeind, T., Huber, R., Dasenbrock, H., Prade, L., and Bieseler, B. (1997) *J. Mol. Biol.* **274,** 446–453
39. Board, P. G., Coggan, M., Chelvanayagam, G., Easteal, S., Jermiin, L. S., Schulte, G. K., Danley, D. E., Hoth, L. R., Griffor, M. C., Kamath, A. V., Rosner, M. H., Chrunyk, B. A., Perregaux, D. E., Gabel, C. A., Geoghegan, K. F., and Pandit, J. (2000) *J. Biol. Chem.* **275,** 24798–24806
40. Chen, H. I., and Sudol, M. (1995) *Proc. Natl. Acad. Sci. U. S. A.* **92,** 7819–7823
41. Wells, W. W., Yang, Y., Deits, T. L., and Gan, Z. R. (1993) *Adv. Enzymol. Relat. Areas Mol. Biol.* **66,** 149–201
42. Kortemme, T., and Creighton, T. E. (1995) *J. Mol. Biol.* **253,** 799–812
43. Bunik, V., Raddatz, G., Lemaire, S., Meyer, Y., Jacquot, J. P., and Bisswanger, H. (1999) *Protein Sci.* **8,** 65–74
44. Suarez-Isla, B. A., Wan, K., Lindstrom, J., and Montal, M. (1983) *Biochemistry* **22,** 2319–2323
45. Sakai, H., and Tsukihara, T. (1998) *J. Biochem. (Tokyo)* **124,** 1051–1059
46. Gilbert, H. F. (1990) *Adv. Enzymol. Relat. Areas Mol. Biol.* **63,** 69–172
47. Klatt, P., and Lamas, S. (2000) *Eur. J. Biochem.* **267,** 4928–4944
48. Stamler, J. S., Toone, E. J., Lipton, S. A., and Sucher, N. J. (1997) *Neuron* **18,** 691–696
49. Cotgreave, I. A., and Gerdes, R. G. (1998) *Biochem. Biophys. Res. Commun.* **242,** 1–9
50. Landry, D. W., Reitman, M., Cragoe, E. J., Jr., and Al-Awqati, Q. (1987) *J. Gen. Physiol.* **90,** 779–798
51. Redhead, C. R., Edelman, A. E., Brown, D., Landry, D. W., and al-Awqati, Q. (1992) *Proc. Natl. Acad. Sci. U. S. A.* **89,** 3716–3720
52. Nicholls, A., Sharp, K. A., and Honig, B. (1991) *Proteins* **11,** 281–296
53. Laskowski, R. A., MacArthur, M. W., Moss, D. S., and Thornton, J. M. (1994) *J. Appl. Crystallogr.* **26,** 283–291
54. Reinemer, P., Prade, L., Hof, P., Neuefeind, T., Huber, R., Zettl, R., Palme, K., Schell, J., Koelln, I., Bartunik, H. D., and Bieseler, B. (1996) *J. Mol. Biol.* **255,** 289–309

Crystal Structure of a Soluble Form of the Intracellular Chloride Ion Channel CLIC1 (NCC27) at 1.4-Å Resolution

Stephen J. Harrop, Matthew Z. DeMaere, W. Douglas Fairlie, Tamara Reztsova, Stella M. Valenzuela, Michele Mazzanti, Raffaella Tonini, Min Ru Qiu, Lucy Jankova, Kristina Warton, Asne R. Bauskin, Wan Man Wu, Susan Pankhurst, Terence J. Campbell, Samuel N. Breit and Paul M. G. Curmi

J. Biol. Chem. 2001, 276:44993-45000.
doi: 10.1074/jbc.M107804200 originally published online September 10, 2001
